RSC Pharmaceutics

ROYAL SOCIETY OF CHEMISTRY

PAPER

View Article Online
View Journal

Cite this: DOI: 10.1039/d5pm00149h

Water mimicry enables the formation of a solid solution of caffeine and theophylline sulphate and a new type of non-stoichiometric hydrate

Enrico Spoletti,[a] Ricardo Albarran Velo,[a] Greta Camilla Magnano,[b] Chiara Cappuccino,[a] Daniel O'Nolan,[a] Lilia Croitor,[a] Dario Voinovich,[b] Beatrice Perissutti[b] and Matteo Lusi*[a]

Received 30th May 2025,
Accepted 19th October 2025

DOI: 10.1039/d5pm00149h

rsc.li/RSCPharma

A solid solution of caffeine and theophylline is realized as sulphate salt hydrate. The molecules enter the structure with one and two equivalents of water, respectively, creating a novel type of non-stoichiometric hydrate. The solid solution is more thermally stable and enables an increased dissolution rate in water for caffeine and theophylline than the respective hydrated sulphate salts. In spite of the increase in solubility, the solid solution shows reduced permeability of caffeine through a synthetic skin membrane when tested against a physical mixture of the parent salts.

Introduction

Solid solutions are multicomponent solid phases in which two or more chemical species can be homogeneously mixed over a range of compositions that is not limited by Daltonian proportions: *i.e.* non-stoichiometric solids. From a structural viewpoint, stoichiometry variability is the result of partial replacement of some molecules or ions with others of similar size, shape and chemical functions (substitutional solid solutions) or by inserting a guest inside structural cavities or pores (interstitial and channel solid solutions, respectively).

For almost 200 years molecular solid solutions (or mixed crystals) have been deemed rare, understudied and treated as a crystallographic curiosity but, thanks to advances in analytical and computational methods, these phases are receiving growing attention.[1] On one hand, they can help in explaining how molecular features translate to certain crystal structures.[2–4] On the other hand, the free combination of multiple molecules into the same phase could enable the formation of materials with desirable properties.[2,5–8] In the pharmaceutical context, substitutional solid solutions can serve to switch stability between different crystal forms and to stabilise metastable polymorphs,[9–11] increasing the solubility and dissolution rate or moisture stability. Additionally, solid solutions enable stoichiometric control in multidrug crystals for precise and personalised dosage.[11–17] Solid solutions are mainly attempted between a limited set of isostructural molecules that form isomorphous crystals.[18] However solid state solubility can be increased though the use of a third component that acts as "solid solvent".[19] Examples of such three-component solid solutions include salts,[20] cocrystals[21] and coordination polymers.[14] Expanding on the supramolecular strategies for the design, synthesis and control of solid solutions would enable their wider exploitation in pharmaceutical and technological applications.[12,20,22,23]

Theophylline (TP) and caffeine (CA) are common stimulant xanthines found in tea leaves and coffee beans. Both molecules are also employed in pharmaceutical therapies. The former is mainly used to treat asthma and chronic obstructive pulmonary disease, and it is administered orally either as a solution, or as a tablet.[24] The latter is used intravenously to prevent and treat apnoea and bronchopulmonary dysplasia in premature babies.[25] Caffeine is administered orally and intranasally as an energy and alertness booster or as an analgesic for a market estimated at over 20 billion USD per year.[26–28] Both molecules are also used transdermally as antiaging cosmetics and extensively investigated as model molecules in chemistry and pharmaceutical science.[29,30] Notably, a portion of theophylline is metabolised to caffeine in the liver.[31] Therefore, they could be regarded as a drug–prodrug pair and their solid solution would enable the evaluation of their synergistic effect into a single solid form.

The molecules have the same backbone structure and only differ in the presence of an additional methyl substituent on the imidazole nitrogen of caffeine (position 7; Fig. 1). Despite the relatively simple structures, they show a very rich crystallography, but no isostructural crystals are observed for the two

[a]Department of Chemical Sciences & Bernal Institute, University of Limerick, Limerick V94 T9PX, Ireland. E-mail: matteo.lusi@ul.ie
[b]Department of Chemical and Pharmaceutical Sciences, University of Trieste, 34127 Trieste, Italy

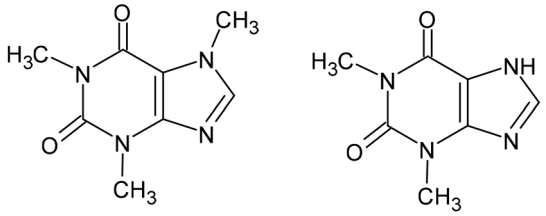

Fig. 1 Chemical structures of caffeine (left) and theophylline (right).

molecules, nor for their salts or cocrystals. Nevertheless, Jones *et al*. obtained a solid solution of CA and TP by freeze-drying;[32] this phase is metastable and readily converts into the 1 : 1 cocrystal form II at ambient temperature, proving the difficult miscibility between the two molecules over a continuous range of composition.

Here full solid state miscibility of the two drugs has been realized *via* a sulphate salt. However, the molecules crystallize with different water contents, producing a fully controllable non-stoichiometric hydrate. The solid solution shows an increased dissolution rate in water for caffeine and theophylline than the physical mixture of the respective hydrated sulphate salts. However, permeability study suggests that the physical mixture of the parent salts enables greater permeation of caffeine in a skin-mimetic membrane compared to the solid solution formulation.

Experimental

Caffeine was purchased from Alfa Aesar (Thermo Scientific Chemicals), theophylline was purchased from Sigma Aldrich and sulfuric acid was purchased from Honeywell Fluka; the reagents were used as received, without further purification.

Solid-state synthesis

Mechanochemical syntheses were performed by manual grinding of the reagents (about 0.5 mmol) in the desired stoichiometric ratios with an agate mortar and pestle in the presence of a stoichiometric amount of diluted H_2SO_4 added with a micropipette. Details are available in the SI.

Solution growth of single crystals

Small amounts (about 0.1–0.3 mmol) of caffeine and theophylline were prepared in the desired stoichiometric ratio and dissolved in ≈4 mL of solvent (synthesis carried out in both water and methanol) in a vial and a stoichiometric amount of diluted H_2SO_4 was added with a micropipette; single crystals formed after a few days by solvent evaporation at room temperature and were analysed by SC-XRD. Details are available in the SI.

Single crystal X-ray diffraction

Data were collected on a Bruker D8 Quest diffractometer equipped with a Mo Kα (λ = 0.71073 Å) radiation source and a Photon 100 detector. The data were integrated with Apex 4. The unit cell parameters for all compounds discussed herein are reported in Table S1. The structures were solved by the intrinsic phasing methods and refined by least-squares methods against F^2 using SHELXT[33] and SHELXL[34] through the OLEX2 interface.[35] Non-hydrogen atoms were refined anisotropically. Hydrogen atoms were placed in calculated positions. The software MERCURY was used for graphic representations.[36]

Powder X-ray diffraction

All diffraction patterns were recorded on a PANalytical EMPYREAN diffractometer system using the Bragg–Brentano geometry and an incident beam of Cu Kα radiation (λ = 1.5418 Å) in the 2θ range between 3° and 40° (step size: 0.013°; time/step: 30 s; Soller slit: 0.04 rad; divergence slit: $\frac{1}{8}$; antiscatter slit: $\frac{1}{4}$; 45 mA X 40 kV). Room temperature scans were performed on a spinning silicon zero-background sample holder.

Variable temperature powder X-ray diffraction

Diffractograms at different temperatures were recorded using a PANalytical X'Pert MPD Pro diffractometer equipped with an X'Celerator detector, operating in scanning line detector mode, and an incident beam of Cu Kα radiation (λ = 1.5418 Å) in the 2θ range between 5° and 40° (step size: 0.0167113°; time/step: 29.845 s; Soller slit: 0.04 rad; divergence slit: $\frac{1}{8}$; antiscatter slit: $\frac{1}{4}$; 40 mA X 40 kV). An Anton Paar TTK 450 stage coupled with an Anton Paar TCU 110 Temperature Control Unit was used to record the variable temperature diffractograms. The powder was loaded on a zero-background sample holder made for the Anton Paar TTK 450 chamber. Measurements were performed under a nitrogen stream between 25 °C and 175 °C, at a 10 °C min^{-1} heating rate.

Thermogravimetric analysis

TGA measurements were performed on TA TGA Q-50 under a nitrogen stream (40 mL min^{-1} for the furnace and 60 mL min^{-1} for the balance) using 4 to 6 mg of ground powder, between room temperature and 300 °C, at a 5 °C min^{-1} heating rate.

Particle size and morphological analysis

The particle size of the solid solution of $CAH^+_{0.5}TPH^+_{0.5}HSO^-_4{\cdot}1.5H_2O$, $CAH^+HSO_4{}^-{\cdot}H_2O$ and $TPH^+HSO_4{}^-{\cdot}2H_2O$ was determined using a Malvern Morphologi G3SE apparatus. A small volume (19 mm^3) of powder was placed into the sample dispersion unit. The powder was dispersed with compressed air on the G3 stage glass. A 5× lens was used (measuring range: 6.5–420 μm) to acquire images of the dispersed sample. Around 500 particles were imaged for each sample. Once scanned, particle parameters were determined with the G3 software with the size reported using the circle equivalent diameter.

The morphology of the powder samples of $CAH^+_{0.5}TPH^+_{0.5}HSO^-_4{\cdot}1.5H_2O$, $CAH^+HSO_4{}^-{\cdot}H_2O$ and

$TPH^+HSO_4^-{\cdot}2H_2O$ was characterized by using a HITACHI SU-70 scanning electron microscope (SEM) instrument. A small amount of the powder was placed onto an adhesive carbon tape previously attached to a cylindrical aluminium 15 mm SEM stub. The samples were coated with gold using an Emitech K550 sputter coater at 20 mA for 40 s. The particles were imaged at a voltage of 10 kV.

Dissolution kinetics

Powder dissolution measurements were conducted in a Grant GD100 water bath at 37.0 °C. Tablets of the solid solution of $CAH^+_{0.5}TPH^+_{0.5}HSO^-_4{\cdot}1.5H_2O$ (0.5 mmol), and a 50 : 50 physical mixture of $CAH^+HSO^-_4{\cdot}H_2O$ and $TPH^+HSO^-_4{\cdot}2H_2O$ (0.5 mmol) were prepared by pressing the powders at two tons for 15 seconds using a Specac hydraulic press. The tablets were placed in a stainless-steel cylindrical mesh basket. The basket was placed in 100 mL of distilled water kept at 37.0 °C under continuous magnetic stirring at 300 rpm (n = 3). The sampling was performed at intervals of 2, 5, 10, 15, 20, 30, 45, and 60 minutes. Withdrawn suspensions were filtered with 0.45 μm syringe filters prior to the injection into the HPLC spectrophotometer. The dissolution aliquots were analysed using a Shimadzu (LC-20A) HPLC instrument with a Gemini® C18 (250 × 4.6 mm 5 μm) column. The wavelength was set to 275 nm; the injection volume was 10 μL with a flow rate of 1 mL min^{-1}; the oven was set at 40 °C. An isocratic mobile phase of 90 : 10 (0.1% orthophosphoric acid in H_2O : 0.1% orthophosphoric acid in acetonitrile) was used.

Permeability measurements

Caffeine permeation from a lipophilic ointment (5% w/w) loaded with either the $CAH^+_{0.50}TPH^+_{0.50}HSO_4^-{\cdot}1.5H_2O$ solid solution or the corresponding 50 : 50 physical mixture of $CAH^+HSO^-_4{\cdot}H_2O$ and $TPH^+HSO^-_4{\cdot}2H_2O$ was performed using diffusion cells and the artificial barriers, namely PermeaPad®, in accordance with OECD guidelines.[37] The PermeaPad® membranes, characterized by specific polarity features, were assembled with the paper filter side facing the donor compartment and the regenerated cellulose side facing the receptor compartment. Both samples were dispersed in a paraffinic lipophilic ointment Pionier PLW Acef (Italy) immediately prior to application onto the membrane, to ensure dispersion of the solid sample rather than its dissolution. The diffusion surface area was 3.14 cm^2. The receptor phase consisted of freshly prepared phosphate-buffered saline (PBS) at pH 7.4, continuously stirred with a Teflon-coated magnetic stirrer. The receptor chamber had an average volume of 15 mL and was filled with receptor fluid. The Franz cells were kept at a controlled temperature of 32 ± 1 °C. At the beginning of the experiment, an infinite dose of 500 mg of the lipophilic ointment was applied directly onto the membrane within the diffusion cell, corresponding to a theoretical dose of Q_0 = 7.96 mg cm^{-2}. The donor compartment was sealed with a parafilm throughout the experiment to prevent evaporation. The permeation study lasted 4 hours to monitor the caffeine diffusion through the barrier or into the skin. At predetermined intervals (0, 15, 30, 45, 60, 120, and 240 minutes), 1.0 mL samples were withdrawn from the receptor compartment and immediately replaced with an equal volume of fresh receptor fluid to maintain sink conditions. All tests were conducted in triplicate. The amount of caffeine in the receptor fluid and in the artificial membranes after 4 hours, was quantified by HPLC.

High-performance liquid chromatography

HPLC measurements were performed on a Agilent 1260 Infinity II system (Agilent Technologies) equipped with a quaternary pump and a Diode Array Detector (DAD) HPLC system (Agilent, Santa Clara, CA, USA). Caffeine separation was performed on a C18 column (Kinetex 5 μm C18 100 Å, 250 × 4.6 mm, Phenomenex, Torrance, CA, USA) maintained at a temperature of 40 °C. The mobile phase consisted of methanol/water (80/20% v/v), delivered in isocratic mode at a flow rate of 1 mL min^{-1}. The injection volume was 20 μL, and the detection wavelength was set at 270 nm. The retention time of caffeine was 2.87 ± 0.02 minutes, and the total run time was 8 minutes. The system was controlled using OpenLab CDS ChemStation Edition software (Agilent, Santa Clara, CA, USA). Before each HPLC analysis, a calibration curve was prepared to calculate the analyte concentration in the collected samples. The caffeine calibration curve was linear over the range of 0.02–0.5 μg mL^{-1} (R^2 = 0.9997), with five calibration points (0; 0.02; 0.04; 0.08; 0.16; and 0.5 μg mL^{-1}).

Results and discussion

Caffeine is reported to form two sulphate salts: an anhydrous form (CCDC refcode HICYEZ)[38] and a monohydrate form ($CAH^+HSO_4^-{\cdot}H_2O$, CCDC refcode AYUBEC),[39] which is isostructural to the theophyllinium hydrogen sulphate dihydrate ($TPH^+HSO_4^-{\cdot}2H_2O$, CCDC refcode OHUQOB) that we have recently reported as part of a solid form screening (Fig. 2).[40]

COMPOUND	Space Group	a (Å)	b (Å)	c (Å)	β (°)
$CAH^+HSO_4^-{\cdot}H_2O$	$P2_1/c$	9.8	6.3	21.3	90.8
$TPH^+HSO_4^-{\cdot}2H_2O$	$P2_1/c$	10.1	6.3	21.6	97.3

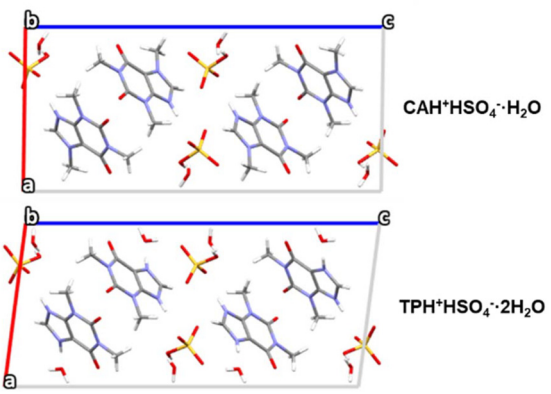

Fig. 2 Unit cell parameters and crystal packing of $CAH^+HSO_4^-{\cdot}H_2O$ and $TPH^+HSO_4^-{\cdot}2H_2O$.

Notably, the caffeine salts show the same thermosalient behaviour reported for theophylline (SI video).[40] In both structures, purine is protonated and one water molecule links three different hydrogen sulphates *via* H-bonds. The additional water molecule in the theophylline salt forms hydrogen bonds with the free imidazole base filling the space occupied by the methyl group in caffeine (Fig. 2).

The isomorphic nature of the two crystals prompted the realization of a solid solution. Slow solvent evaporation of purine solutions in either water or methanol with sulfuric acid yields single crystals suitable for structural characterization. X-ray diffraction analysis confirms the presence of both molecules in a homogeneous solid solution of $CAH^{+}_{1-x}TPH^{+}_{x}HSO_4^{-}\cdot(1+x)H_2O$ and a stoichiometry variation is observed across multiple crystals obtained at different caffeine–theophylline ratios (Fig. 3a, Table S1). In the solid solution, the methyl group of the caffeine is replaced by a water molecule H-bonded to the protonated nitrogen (N7) of theophylline. Hence, N7–H···OH_2 takes the place of the covalent bond N7–C14 (Fig. 3b).

The different water stoichiometry in the pure salts translates into a solid solution in which the water content varies with composition. Such solid solution differs from more common non-stoichiometric hydrates in which water molecules can freely fill structural voids (channels or pockets).[41–45] In the pharmaceutical industry the latter pose serious formulation issues as their composition may vary with temperature and humidity, affecting the integrity of the drug product.[46–48] In contrast, in the caffeine–theophylline system the stoichiometry of the hydrate is linked to the relative amount of the drug molecules.

The same solid solution is produced mechanochemically, by liquid assisted grinding, as a uniform polycrystalline powder (Fig. 4 and Fig. S1) and it is stable for over a year when stored under ambient conditions (Fig. S2).

The salts dehydrate on heating between 50 and 70 °C, with the solid solutions being more stable than the pure forms (see TGA in Fig. 5). Dehydration by heating causes a phase separation into the two anhydrous salts $TPH^{+}HSO_4^{-}$ form II (CSD refcode OHUQAN03)[40] and $CAH^{+}HSO_4^{-}$ (CSD refcode HICYEZ)[38] (see VT-PXRD in Fig. S3). Notably, the non-stoichiometric hydrate is restored upon exposure to air (Fig. S4), perhaps *via* the formation of a liquid intermediate that allows the necessary ion mobility.[49,50]

Caffeine and theophylline belong to class I of the biopharmaceutics classification system and are soluble in water.

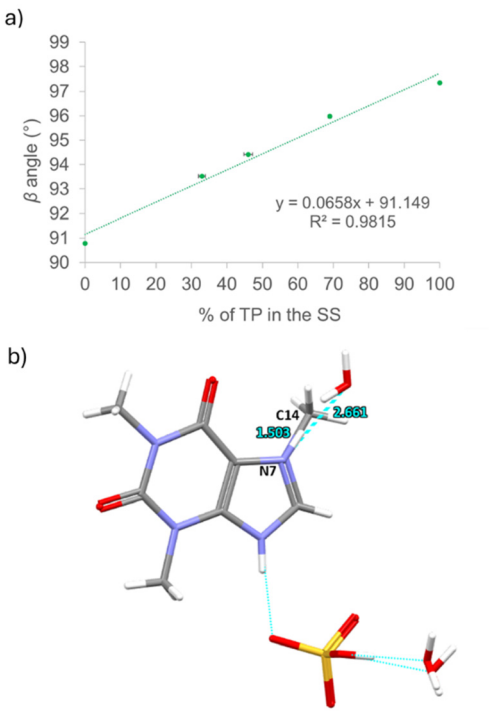

Fig. 3 (a) Linear dependence between the β angle and the percentage of TP present in the solid solution of $CAH^{+}_{1-x}TPH^{+}_{x}HSO_4^{-}\cdot(1+x)H_2O$. (b) Asymmetric unit for the solid solution of $CAH^{+}_{0.54}TPH^{+}_{0.46}HSO_4^{-}\cdot1.46H_2O$ showing the length of the covalent bond N7–C14 and the H-bond N7–H···OH_2; H-bonds are presented as cyan dashed lines.

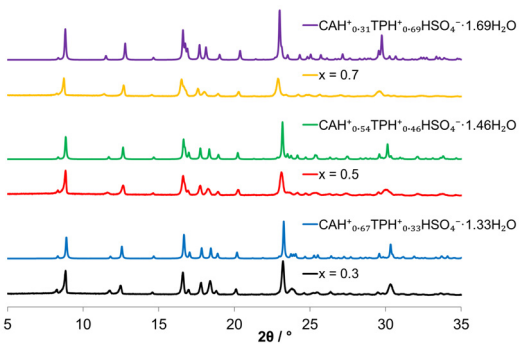

Fig. 4 Comparison of experimental PXRD patterns for the product of the liquid assisted grinding of CA/TP mixtures $CA_{1-x}TP_x$ with x = 0.30, 0.50, 0.70 in the presence of a stoichiometric amount of H_2SO_4 and the calculated patterns of the solid solution of $CAH^{+}_{1-x}TPH^{+}_{x}HSO_4^{-}\cdot(1+x)H_2O$ obtained from single crystal X-ray diffraction analyses.

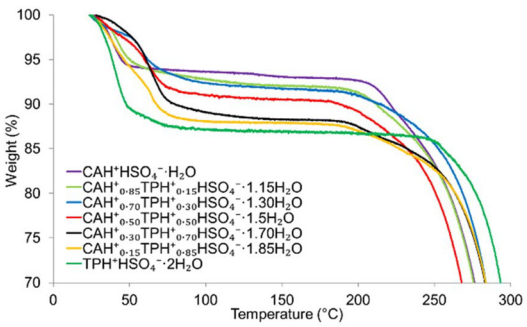

Fig. 5 TGA analysis of the solid solution $CAH^{+}_{1-x}TPH^{+}_{x}HSO^{-}_{4}\cdot(1+x)H_2O$ with x = 0.15, 0.30, 0.50, 0.70, 0.85 and for $CAH^{+}HSO_4^{-}\cdot H_2O$ and $TPH^{+}HSO_4^{-}\cdot2H_2O$.

However, the solid solution of $CAH^{+}_{1-x}TPH^{+}_{x}HSO^{-}_{4}\cdot(1+x)H_2O$ manifests an increased dissolution rate of CA and TP in water with respect to the 50 : 50 physical mixture of the respective hydrated sulphate salts ($CAH^{+}HSO_4^{-}\cdot H_2O$: $TPH^{+}HSO_4^{-}\cdot 2H_2O$, Fig. 6), in spite of having larger particle size (Table S2). This is a common behaviour of solid solutions and likely due to less favourable packing energy of the mixed crystal.

The potential benefit of the solid solution for topical application was evaluated in an artificial skin. Permeation of caffeine was tested from a lipophilic ointment (5% w/w) loaded with either the $CAH^{+}_{0.50}TPH^{+}_{0.50}HSO_4^{-}\cdot 1.5H_2O$ solid solution or the corresponding 50 : 50 physical mixture $CAH^{+}HSO^{-}_{4}\cdot H_2O$: $TPH^{+}HSO^{-}_{4}\cdot 2H_2O$ using the PermeaPad® barrier. The concentration of caffeine measured in the receiving phase (Fig. 7) allows for the evaluation of the actual amount of the compound that crosses the membrane and can be systemically absorbed.

The physical mixture enables grater permeation of caffeine than the solid solution formulation, reaching average values of 0.86 ± 0.12% and 0.43 ± 0.05% of caffeine released at the end of the test (4 hours), respectively. Notably, the release profiles of the two formulations are very similar during the initial intervals; however, a divergence became significantly evident toward the end of the experiment: the solid solution appeared to approach a plateau after 4 hours, suggesting a possible saturation or a controlled release mechanism; the physical mixture continued to show a gradual increase, indicating a less sustained release profile. These findings suggest that the matrix structure and the solid form of caffeine within the formulation may significantly influence the release profiles. Moreover, the retention of the caffeine in the entire membrane was also quantified and is presented in Fig. 8. Caffeine accumulation in the Permeapad® membrane was significantly higher when the physical mixture was used, compared to the solid solution, reaching a mean value of 1.75 ± 0.37% and 0.34 ± 0.14%, respectively. The reduced permeability of the solid solution and its lower accumulation into the membrane is counterintuitive. Perhaps, despite the higher water solubility, the presence of the theophylline ions with their additional H-bonds translates into a lower solubility of the solid solution in the lipophilic ointment, which would reduce the fraction of free caffeine available for partitioning into the membrane. In the physical mixture, these interactions are less pronounced, resulting in a higher effective activity of caffeine at the vehicle–membrane interface. This hypothesis aligns with previous reports on transdermal delivery, where the thermodynamic activity of the drug within the vehicle is a key determinant of uptake, suggesting that differences in activity, rather than protonation/deprotonation of the molecule, are responsible for the differential accumulation.[51,52]

Furthermore, the choice of the delivery vehicle is critical: incorporating physical mixtures and solid solutions into a water base gel would result in full solubilization of both, effectively leading to the evaluation of two structurally equivalent systems. In contrast, when dispersed in the lipophilic ointment (petrolatum-based), the two systems remain structurally distinct, allowing for the preservation of their individual characteristics. However, the general trend observed here—higher accumulation in the physical mixture—is consistent with mechanistic expectations based on drug activity and molecular interactions and may be relevant for other semisolid vehicles.

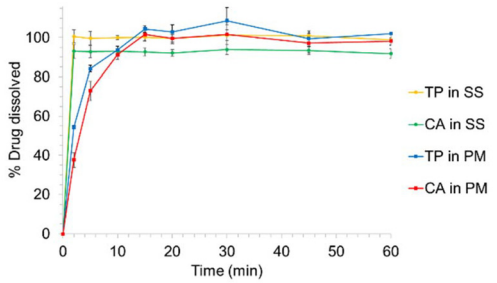

Fig. 6 Tablet dissolution experiments performed for the solid solution (SS) of $CAH^{+}_{0.5}TPH^{+}_{0.5}HSO^{-}_{4}\cdot 1.5H_2O$ (CA: green line, TP: yellow line) and the 50 : 50 physical mixture (PM) of $CAH^{+}HSO_4^{-}\cdot H_2O$ and $TPH^{+}HSO_4^{-}\cdot 2H_2O$ (CA: red line, TP: blue line); the dissolution experiment was conducted in 100 ml of distilled water using a stirring speed of 300 rpm at 37.0 °C.

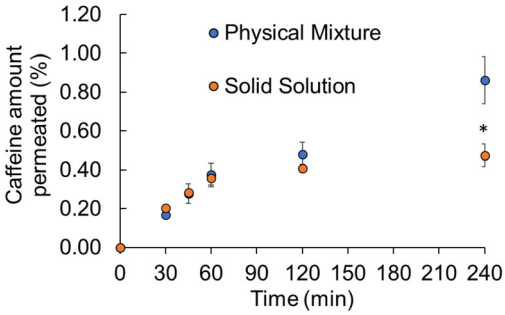

Fig. 7 Permeation profile of the caffeine lipophilic ointment formulation that permeated in the receptor fluid at specific extraction times through PermeaPad®. Values are expressed as mean ± standard error of the mean (SEM) (n = 3). * Denotes statistically significant differences between the solid solution and physical mixture ($p < 0.05$).

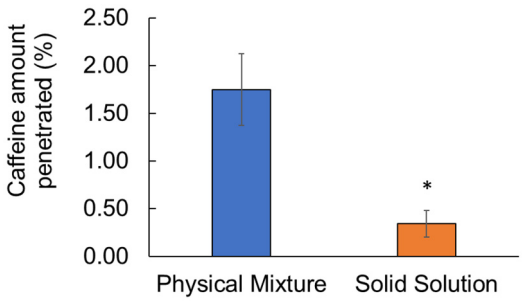

Fig. 8 Distribution of caffeine lipophilic ointment formulations in the entire PermeaPad® barrier. Values are expressed as mean ± standard error of the mean (SEM) (n = 3). * Denotes statistically significant differences between the solid solution and physical mixture ($p < 0.05$).

Finally, the use of the artificial membrane allows a controlled and reproducible assessment of partitioning, though it lacks metabolic clearance or vascular transport. Therefore, while absolute permeation values may differ *in vivo*, the relative differences between the physical mixture and the solid solution provide valuable insights into formulation-dependent transdermal delivery.

Conclusions

In summary, caffeine and theophylline can be mixed in a solid solution through salification with sulfuric acid. The differences in the molecular structure are overcome by the presence of a water molecule that occupies the space of the methyl group in the caffeine while satisfying the requirement for a H-bond acceptor for the imidazole donor in theophylline.

Beyond marginal gains in thermal stability and dissolution rate, the reported solid solution allows precise stoichiometric control of two molecules with a potential synergistic effect into a uniform crystalline phase for precise and personalised dosage. Additionally, a permeability test shows that the different solid forms affect the drug transport and accumulation in a synthetic membrane and confirm that solid solutions can be formulated to alter the permeability of drugs for topical administration.

Finally, from a chemical and crystallography standpoint, the mimicry behaviour of water could enable the design and realization of other non-stoichiometric crystals between pairs of N-heteroaromatic bases and their *N*-methylated analogues expanding the scope of solid solutions.

Conflicts of interest

There are no conflicts to declare.

Data availability

The data supporting this article have been included as part of the supplementary information (SI). Supplementary information: experimental details, PXRD and VTPXRD and crystallographic data. See DOI: https://doi.org/10.1039/d5pm00149h.

CCDC 2444505–2444507 contain the supplementary crystallographic data for this paper.[53a–c]

Acknowledgements

E. S. and M. L. thank The Bernal Institute, Boston Scientific, Department of Chemical Sciences and the University of Limerick Foundation for the funding support enabling this research through the mULtiply program.

References

1 M. Lusi, *CrystEngComm*, 2018, **20**, 7042–7052.
2 M. Lusi, *Cryst. Growth Des.*, 2018, **18**, 3704–3712.
3 A. Hill, W. Kras, F. Theodosiou, M. Wanat, D. Lee and A. J. Cruz-Cabeza, *J. Am. Chem. Soc.*, 2023, **145**, 20562–20577.
4 D. Braun and U. Griesser, *CrystEngComm*, 2017, **19**, 3566–3572.
5 M. K. Mishra, U. Ramamurty and G. R. Desiraju, *J. Am. Chem. Soc.*, 2015, **137**, 1794–1797.
6 E. Engler, B. Scott, S. Etemad, T. Penney and V. Patel, *J. Am. Chem. Soc.*, 1977, **99**, 5909–5916.
7 M. Morimoto, S. Kobatake and M. Irie, *J. Am. Chem. Soc.*, 2003, **125**, 11080–11087.
8 T. Fukushima, S. Horike, Y. Inubushi, K. Nakagawa, Y. Kubota, M. Takata and S. Kitagawa, *Angew. Chem., Int. Ed.*, 2010, **49**, 4820–4824.
9 W. Kras, A. Carletta, R. Montis, R. A. Sullivan and A. J. Cruz-Cabeza, *Commun. Chem.*, 2021, **4**, 38.
10 D. H. Case, V. K. Srirambhatla, R. Guo, R. E. Watson, L. S. Price, H. Polyzois, J. K. Cockcroft, A. J. Florence, D. A. Tocher and S. L. Price, *Cryst. Growth Des.*, 2018, **18**, 5322–5331.
11 E. Spoletti, V. Verma, C. Cappuccino and M. Lusi, *Chem. Commun.*, 2023, **59**, 14321–14324.
12 V. Verma, S. Bordignon, M. R. Chierotti, M. Lestari, K. Lyons, L. Padrela, K. M. Ryan and M. Lusi, *IUCrJ*, 2020, **7**, 1124–1130.
13 C. Cappuccino, E. Spoletti, F. Renni, E. Muntoni, J. Keiser, D. Voinovich, B. Perissutti and M. Lusi, *Mol. Pharm.*, 2023, **20**, 2009–2016.
14 M. Lestari, M. Lusi, A. O'Leary, D. O'Nolan and M. J. Zaworotko, *CrystEngComm*, 2018, **20**, 5940–5944.
15 D. E. Braun, V. Kahlenberg and U. J. Griesser, *Cryst. Growth Des.*, 2017, **17**, 4347–4364.
16 J. D. C. Fonseca, J. C. Tenorio Clavijo, N. Alvarez, J. Ellena and A. P. Ayala, *Cryst. Growth Des.*, 2018, **18**, 3441–3448.
17 K. H. Kim and C. I. Jarowski, *J. Pharm. Sci.*, 1977, **66**, 1536–1540.
18 A. I. Kitaigorodsky, *Mixed crystals*, Springer Science & Business Media, 2012.
19 M. Lusi, I. J. Vitorica-Yrezabal and M. J. Zaworotko, *Cryst. Growth Des.*, 2015, **15**, 4098–4103.
20 M. Lestari and M. Lusi, *Chem. Commun.*, 2019, **55**, 2297–2300.
21 M. A. Oliveira, M. L. Peterson and D. Klein, *Cryst. Growth Des.*, 2008, **8**, 4487–4493.
22 E. Schur, E. Nauha, M. Lusi and J. Bernstein, *Chem. – Eur. J.*, 2015, **21**, 1735–1742.
23 A. J. Cruz-Cabeza, M. Lestari and M. Lusi, *Cryst. Growth Des.*, 2018, **18**, 855–863.
24 P. J. Barnes, *Pharmaceuticals*, 2010, **3**, 725–747.
25 B. Schmidt, R. S. Roberts, P. Davis, L. W. Doyle, K. J. Barrington, A. Ohlsson, A. Solimano and W. Tin, *N. Engl. J. Med.*, 2006, **354**, 2112–2121.

26 A. Herman and A. Herman, *Skin Pharmacol. Physiol.*, 2012, **26**, 8–14.
27 R. R. McCusker, B. A. Goldberger and E. J. Cone, *J. Anal. Toxicol.*, 2006, **30**, 112–114.
28 C. J. Derry, S. Derry and R. A. Moore, *Cochrane database of systematic reviews*, 2014.
29 M. Bertolini, Y. Ramot, J. Gherardini, G. Heinen, J. Chéret, T. Welss, M. Giesen, W. Funk and R. Paus, *Int. J. Cosmet. Sci.*, 2020, **42**, 79–88.
30 A. Herman and A. P. Herman, *Skin Pharmacol. Physiol.*, 2012, **26**, 8–14.
31 T. J. Haley, *Drug Metab. Rev.*, 1983, **14**, 295–335.
32 M. D. Eddleston, B. Patel, G. M. Day and W. Jones, *Cryst. Growth Des.*, 2013, **13**, 4599–4606.
33 G. M. Sheldrick, *Acta Crystallogr., Sect. A: Found. Adv.*, 2015, **71**, 3–8.
34 G. M. Sheldrick, *Acta Crystallogr., Sect. C: Struct. Chem.*, 2015, **71**, 3–8.
35 O. V. Dolomanov, L. J. Bourhis, R. J. Gildea, J. A. K. Howard and H. Puschmann, *J. Appl. Crystallogr.*, 2009, **42**, 339–341.
36 C. F. Macrae, I. Sovago, S. J. Cottrell, P. T. A. Galek, P. McCabe, E. Pidcock, M. Platings, G. P. Shields, J. S. Stevens, M. Towler and P. A. Wood, *J. Appl. Crystallogr.*, 2020, **53**, 226–235.
37 T. G. OECD, *OECD Guidelines for the Testing of Chemicals, Section*, 2004, vol. 4.
38 C. Mottillo, Y. Lu, M.-H. Pham, M. J. Cliffe, T.-O. Do and T. Friščić, *Green Chem.*, 2013, **15**, 2121–2131.
39 C. V. Jerin and S. Athimoolam, *Struct. Rep.*, 2011, 67, o2290–o2290.
40 E. Spoletti, R. Albarran Velo, C. Phelan, C. Williams and M. Lusi, *Cryst. Growth Des.*, 2024, **25**, 330–339.
41 U. J. Griesser, *Polymorphism: In the pharmaceutical industry*, 2006, pp. 211–233.
42 S. R. Vippagunta, H. G. Brittain and D. J. Grant, *Adv. Drug Delivery Rev.*, 2001, **48**, 3–26.
43 J.-R. Authelin, *Int. J. Pharm.*, 2005, **303**, 37–53.
44 S. M. Reutzel and V. A. Russell, *J. Pharm. Sci.*, 1998, **87**, 1568–1571.
45 M. F. Pina, J. O. F. Pinto, J. J. Sousa, L. Fabian, M. Zhao and D. Q. Craig, *Mol. Pharm.*, 2012, **9**, 3515–3525.
46 S. M. Reutzel-Edens, D. E. Braun and A. W. Newman, *Polymorphism in the Pharmaceutical Industry: Solid Form and Drug Development*, 2018, pp. 159–188.
47 D. E. Braun and U. J. Griesser, *Cryst. Growth Des.*, 2016, **16**, 6111–6121.
48 D. E. Braun, L. H. Koztecki, J. A. McMahon, S. L. Price and S. M. Reutzel-Edens, *Mol. Pharm.*, 2015, **12**, 3069–3088.
49 D. Chen, G. Haugstad, Z. J. Li and R. Suryanarayanan, *J. Pharm. Sci.*, 2010, **99**, 4032–4041.
50 E. Spoletti, M. O. Diniz, M. Svärd, Å. Rasmuson, S. P. Hudson and M. Lusi, *Chem. – Eur. J.*, 2025, **31**, e202403488.
51 H. G. Brittain, in *Analytical Profiles of Drug Substances and Excipients*, ed. H. G. Brittain, Academic Press, 2002, vol. 29, pp. 1–5.
52 G. Jourquin and J.-M. Kauffmann, *J. Pharm. Biomed. Anal.*, 1998, **18**, 585–596.
53 (*a*) CCDC 2444505: Experimental Crystal Structure Determination, 2025, DOI: 10.5517/ccdc.csd.cc2n1q0g; (*b*) CCDC 2444506: Experimental Crystal Structure Determination, 2025, DOI: 10.5517/ccdc.csd.cc2n1q1h; (*c*) CCDC 2444507: Experimental Crystal Structure Determination, 2025, DOI: 10.5517/ccdc.csd.cc2n1q2j.